



Investigation of split CoFeB/Ta/CoFeB/MgO stacks for magnetic memories applications



ARTICLE INFO

Keywords:

Perpendicular magnetic anisotropy
Spin-orbit torques
MRAMs
CoFeB
W underlayers

ABSTRACT

We report on the static and dynamic magnetic properties of W/CoFeB/Ta/CoFeB/MgO stacks, where the CoFeB layer is split in two by a 0.3 nm-thick Ta “dusting” layer. A total CoFeB thickness between 1.2 and 2.4 nm is studied. Perpendicular magnetic anisotropy is obtained for thickness below 1.8 nm even at the as-deposited stacks, and it is enhanced after annealing. Saturation magnetization is 1520 (1440) kA/m before (after) annealing, increased compared to non-split CoFeB layers. Ferromagnetic resonance measurements show that high magnetic anisotropy energy may be achieved (effective anisotropy field 0.571 ± 0.003 T), combined to a moderate Gilbert damping (0.030 ± 0.001). We argue that the above characteristics make the split-CoFeB system advantageous for spintronics applications.

1. Introduction

Recently, W-based spin-Hall devices and magnetic tunnel junctions (MTJs) have been the subject of several studies [1–4] due to their importance for magnetic memory and logic applications. The principal focus has been on the study of CoFeB/MgO/CoFeB stacks, the current MTJ industry standard [5], grown on W underlayers. The emergence of spin-orbit torque magnetic random access memory (SOT-MRAM) [6–9] is driving much of this interest, as the high spin-orbit coupling coefficient of the β crystallographic phase of W [10]. A requirement for implementing SOT-MRAM is the realization of a heavy-metal/ferromagnetic-metal bilayer for performing SOT-induced magnetization switching. Additionally, W-based MTJs have shown superior thermal stability than the ones grown on the standard Ta underlayer [11–14], allowing for improving the performance of spin-transfer torque MRAMs and magnetic field sensors.

Another requirement for SOT-MRAM applications is perpendicular magnetic anisotropy (PMA) [5]. Although CoFeB/MgO bilayers readily obtain PMA when grown onto Ta [5], this is not the case for W. Initial studies showed that PMA can be obtained by inserting an intermediate layer between W and CoFeB, e.g. Hf [15] or Ta [16]; however, these elements have lower spin-orbit coupling than β -W. Recently, W/CoFeB/MgO stacks with PMA have been obtained, although tedious processing is required, including long annealing runs in applied magnetic field, or rapid thermal annealing [2,3,11,17]. Furthermore, PMA is obtained in split-CoFeB layers (two CoFeB layers separated by an intermediate layer) [18–20], although in none of the reported cases the stacks were grown on W. It should be noted that split-ferromagnetic layers using heavy-metal spacers have been recently employed for creating synthetic anti-ferromagnets (SAFs) having PMA; these concern CoFeB/Ta/CoFeB [21] and Co/Ru/Co/Pt [22] stacks that take advantage of SOTs arising at the top and bottom heavy-metal spacer interfaces for magnetization switching. This approach is of technological importance since SAFs are

extensively employed as reference layers in MTJs; on the contrary, in our approach the focus is to exploit the high SOTs at the W/split-CoFeB interface.

In this work we study split CoFeB/Ta/CoFeB stacks grown directly onto W. Ta is an efficient B getter, contributing to the crystallization of the amorphous as-deposited CoFeB layer into the body-centered cubic (0 0 1) structure of the MgO (0 0 1) layer, ultimately giving rise to high interface anisotropy [23]. The samples studied in this work were magnetron sputtered W (6 nm)/Co₂₀Fe₆₀B₂₀ (*t* nm)/Ta (0.3 nm)/Co₂₀Fe₆₀B₂₀ (*t* nm)/MgO (2 nm) stacks; we have also studied split-CoFeB stacks with a 0.6 nm thick Ta “dusting” layer; however, the obtained results are less promising (see “Supplementary Material”).

2. Material and methods

Sample deposition was carried out in an ultra-high vacuum (base pressure 1.5×10^{-9} Torr) magnetron sputtering system (AJA ATC-2200-V) in diode configuration.¹ Commercially available Si (1 0 0) substrates covered with an amorphous 500 nm thick thermal SiO₂ were used. Each magnetic multilayered film sample additionally had a 5 nm thick AlO_x capping layer to prevent oxygen diffusion through MgO and into CoFeB. A direct current (radio frequency) power supply was used for metal (oxide) deposition, at 1.5 W/cm^2 (10 W/cm^2) power density and 3 mTorr Ar working pressure, leading to 0.018 nm/s (0.010 nm/s) deposition rate. The substrate was rotated during deposition (80 revolutions per minute) for avoiding the emergence of any in-plane magnetic anisotropy axes. After deposition the samples were annealed for 1 h at 350 °C in an auxiliary vacuum chamber (pressure during annealing better than $1 \cdot 10^{-5}$ Torr). The ramp-up rate was controlled at 20 °C/min, while the films were allowed to cool down to room temperature with the heating element turned off in high vacuum before removal. We have previously shown [24,25] that W retains the desired β -phase through the above mentioned annealing process.

¹ Certain equipment, instruments or materials are identified in this paper in order to adequately specify the experimental details. Such identification does not imply recommendation by the co-authors nor does it imply the materials are necessarily the best available for the purpose.

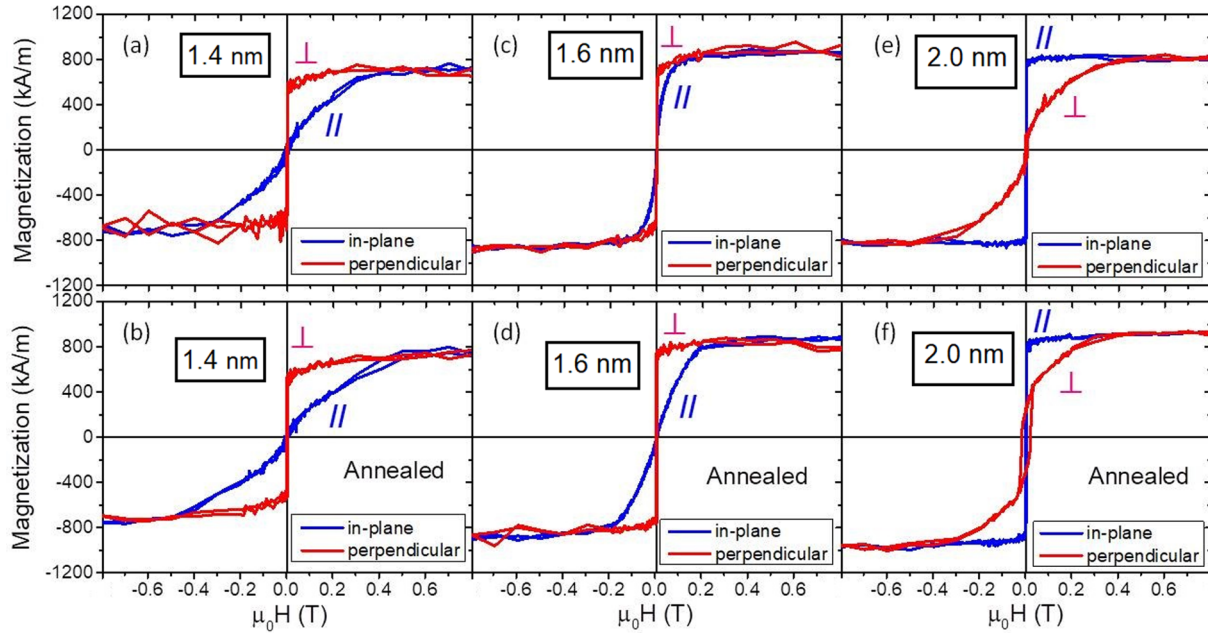


Fig. 1. Representative set of hysteresis loops before (top) and after (bottom) annealing for t_T equal to 1.4 nm (a) and (b), 1.6 nm (c) and (d), and 2.0 nm (e) and (f).

3. Results and discussion

3.1. Magnetostatic properties

Samples with t varying from 0.6 to 1.2 nm, equal to a total CoFeB thickness (t_T) from 1.2 to 2.4 nm, have been studied. The in-plane and perpendicular magnetization values versus the applied magnetic field have been recorded using vibrating sample magnetometry (VSM), and a representative set of hysteresis loops, before and after annealing, is shown in Fig. 1 (see “Supplementary Material” for the rest of the data). The striking characteristic is that PMA is obtained even at the as-deposited samples, up to t_T equal 1.6 nm. Upon annealing, the anisotropy field H_k (defined as the hard-axis saturation field and measured at the intersection of the in-plane and perpendicular to the plane loops) increases, indicating a corresponding PMA energy increase. When t_T equals 2.0 nm, the easy magnetization axis lies in the plane of the stacks, even after annealing. Thus, the PMA to in-plane magnetic anisotropy (IMA) transition occurs between a CoFeB thickness of 1.6 and 2 nm. PMA is also obtained when a 0.6 nm thick Ta “dusting” layer is used, for t_T 1.2, 1.4, and 1.6 nm (see “Supplementary Material”); however, saturation magnetization (M_S) is significantly lower. Furthermore, in our previous study [16] we have shown that samples with no Ta addition, processed using the same experimental conditions, do not show PMA at any CoFeB thickness. According to the literature, a major contribution to PMA in this system comes from the CoFeB/MgO interface [5]; particularly, the as-deposited amorphous CoFeB/MgO stack coherently crystallizes to the bcc (001) crystal structure, resulting in high CoFeB/MgO interface anisotropy and the observed PMA. Thus, the PMA to IMA transition observed is a result of the prevalence of the CoFeB layer shape anisotropy at higher thicknesses over the CoFeB/MgO interface anisotropy.

The effective magnetic anisotropy energy (K_{eff}) of the stacks is determined using the relation:

$$K_{eff} = K_V + \frac{K_S}{t_T} \quad (1)$$

where K_V is the volume anisotropy energy and K_S is the MgO/CoFeB interface anisotropy energy (one interface is considered) [26]. K_{eff} is negative (positive) for IMA (PMA) and is determined experimentally from $K_{eff} = H_k M_S / 2$ [16]. Fig. 2a shows the plot of the product $K_{eff} t_T$

versus t_T . Dashed lines represent linear fits to the data (excluding the points that correspond to 1.2 nm CoFeB thickness); the vertical axis intercept equals to K_S , whereas the slope gives K_V . The obtained K_S values are 1.6 ± 0.1 mJ/m² as-deposited and 1.8 ± 0.3 mJ/m² after annealing, comparable to the ones reported in the literature for CoFeB/MgO stacks deposited on W [3,12] and Hf or Ta [18].

The saturation magnetic moment (m_S) per surface area versus t_T plot (shown in Fig. 2b) allows for determining M_S and the magnetic dead-layer thickness (t_d); linear fits to the data yield M_S from the slope and t_d from the y-axis intercept. The obtained M_S and t_d values are 1520 ± 169 kA/m and 0.72 ± 0.12 nm before annealing and 1440 ± 75 kA/m and 0.70 ± 0.09 nm after annealing, showing that the M_S and t_d remain relatively unchanged. It should be noted that this trend is in contrast to previous reports on the annealing effect on the magnetization of MgO/CoFeB/Ta stacks [27], where a clear increase of M_S after annealing at 350 °C is obtained. In addition, a wide scattering of t_d values has been reported in previous studies, both for Ta/CoFeB/MgO and W/CoFeB/MgO: some indicate the existence of a large t_d , up to 0.7 nm after annealing in 350 °C [12,28] and others report negligible t_d [29]. The above indicate the significant dependence of the magnetostatic properties of the stacks to their design.

In our previous study of W/Ta/CoFeB/MgO stacks, performed using identical deposition conditions [16], when a 0.3 nm thick Ta layer was used, t_d equaled 0.3 nm after annealing at 350 °C; however, in that case PMA was obtained only up to 0.9 nm of CoFeB thickness. On the other hand, when a 1 nm thick Ta layer was used, t_d equaled 0.7 nm after annealing at 350 °C and PMA was obtained up to a CoFeB thickness of 1.4 nm. However, the W/Ta/CoFeB/MgO stack yield M_S equal to 1200 kA/m, whereas the split-CoFeB stack has M_S equal to 1440 kA/m. This is a clear advantage of the split-CoFeB design compared to the W/Ta/CoFeB/MgO design, as CoFeB layers with higher M_S result in higher spin-polarization in MTJs.

3.2. Dynamic magnetic properties

Broadband FMR spectroscopy measurements using a signal generator and a microwave diode detector were carried out on two split-CoFeB stacks, annealed at 350 °C, with t_T equal 1.4 and 2.0 nm (PMA and IMA, respectively). For comparison purposes, annealed W/Ta/CoFeB/MgO stacks were also measured (see “Supplementary

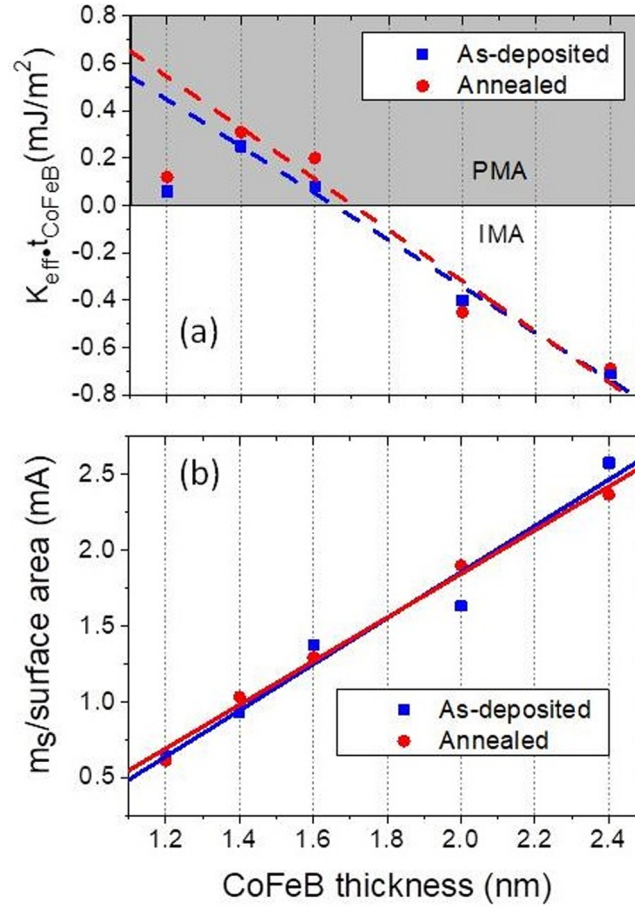


Fig. 2. (a) Dependence of $k_{\text{eff}}t_{\text{CoFeB}}$ as a function of t_T ; dashed lines represent linear fits to the data. (b) Magnetic moment per surface area versus total CoFeB thickness; solid lines represent linear fits to the data.

Material”), with CoFeB thickness of 1.4 and 1.8 nm (PMA and IMA, respectively). To increase the ferromagnetic resonance sensitivity, the external magnetic field was modulated and a lock-in detection scheme was used, whereby FMR spectra were measured at fixed microwave frequencies (in the range 2 GHz–45 GHz) under a swept external magnetic field.

To detect higher-order anisotropies and to address asymmetry in the Landé- g factor, FMR measurements were performed in both the in-plane and out-of-plane geometries. Fig. 3(a) shows illustrative FMR measurements for out-of-plane fields for the 1.4 nm split CoFeB layer from which we extract the frequency-dependent resonance field and the linewidth ΔH . The solid red lines reflect the best-fit of the raw absorption data (unshaded markers) to a derivative Lorentzian absorption line. Expressions for the in-plane (out-of-plane) frequency versus applied field dispersion are given by the Kittel equation [30]:

$$f_{\parallel}^2 = \left(\frac{g^{\parallel} \mu_B \mu_0}{h} \right)^2 H(H - H_{\text{eff}}^{\parallel}), \quad (2)$$

$$f_{\perp} = \frac{g^{\perp} \mu_B}{h} (H + H_{\text{eff}}^{\perp}), \quad (3)$$

for which $f_{\perp}^{(0)}$, $g^{\perp(0)}$, $H_{\text{eff}}^{\perp(0)}$ are the out-of-plane (in-plane) ferromagnetic resonance frequency, Landé- g factor and effective anisotropy field, respectively, h is the Planck constant and μ_0 is the vacuum permeability. The effective anisotropy field values in the Kittel equation are dependent on the second- and fourth-order uniaxial anisotropy coefficients K_2 , K_4 : $H_{\text{eff}}^{\perp} = 2K_2/\mu_0 M_S - M_S + 2K_4/\mu_0 M_S$, and $H_{\text{eff}}^{\parallel} = 2K_2/\mu_0 M_S - M_S$, whereby the fourth-order anisotropy presents itself through the discrepancy in the estimated anisotropy field for in-

plane and out-of-plane FMR. Curve fitting of the resonance field versus frequency graphs (shown in Fig. 3(b and c) yield the magnetic anisotropy field and gyromagnetic ratio (g -factor) values, whereas fitting of the linewidth versus frequency (Fig. 3(d)) yields the Gilbert damping factor α . The Gilbert damping and inhomogeneous broadening of the 2.0 nm split CoFeB layer was extracted from linear fits to the frequency range above 20 GHz, as the non-linear behavior below 20 GHz reflects additional low-frequency losses leading to increases in the inhomogeneous linewidth broadening [31,32]. We exclusively use the out-of-plane measurements to estimate α to exclude two-magnon contributions to the linewidth. The obtained values are listed in Table 1.

The 2.0 nm thick split-CoFeB layer (with IMA) has g factor (2.10) close to the bulk Fe value (2.08) and even closer to the value of a 20 nm thick single-crystalline Fe-rich CoFe alloy thin film (2.09) [33]. Furthermore, the isotropic (perpendicular and in-plane) g factor suggests that most of the orbital moment is quenched, typical of crystal lattices. On the contrary, a marked anisotropy in the Landé- g factor is observed for the split 1.4 nm thick PMA sample (2.22 perpendicular versus 1.94 in-plane), which has been previously understood in terms of a large out-of-plane orbital moment [34]. Indeed, both 1.4 nm samples (split and single layer) exhibit PMA and the corresponding g -factor asymmetry, indicative of the enhanced out-of-plane orbital moment associated with the broken symmetry at the surface and interfaces.

Gilbert damping shows an intense decrease as thickness increases (α is 0.030 at the 1.4 nm thick split-CoFeB layer and 0.022 at the 2.0 nm thick one), in agreement to a previous study of Ta/CoFeB/MgO stacks [5], where α decreases from 0.027 to 0.010, as the CoFeB thickness increases from 1.3 nm to 2.0 nm. It should be noted that the overall higher α value reported here could be attributed to the presence of the

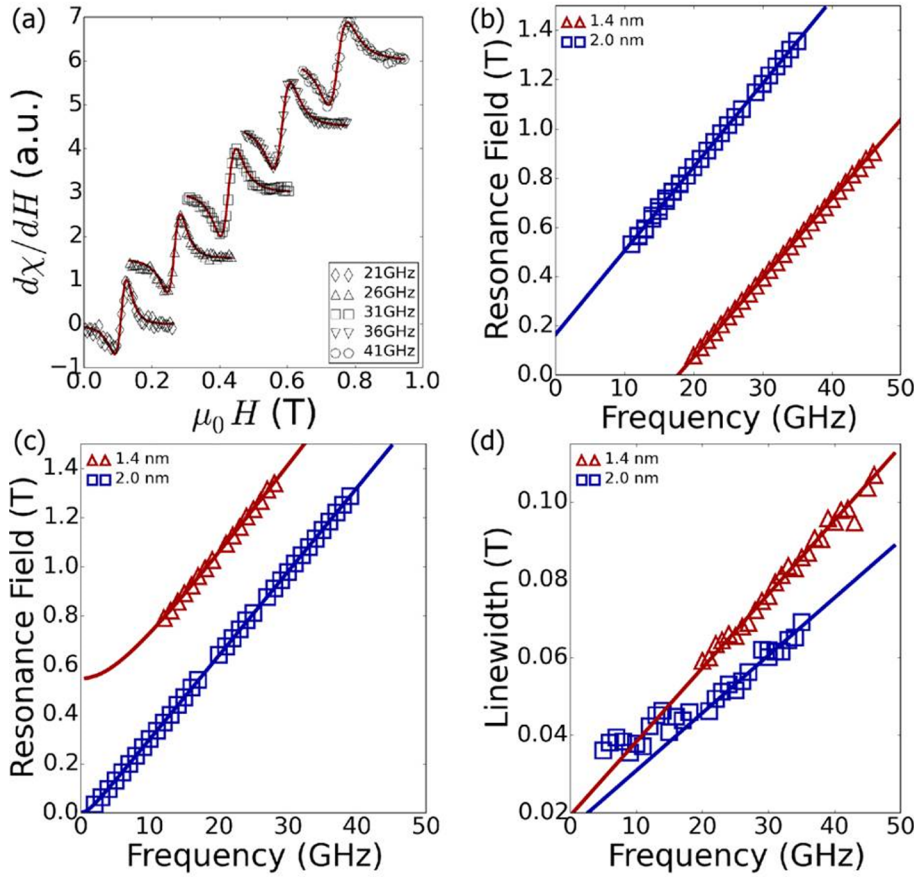


Fig. 3. (a) A sample of the measured ferromagnetic resonance spectra of a 1.4 nm split CoFeB layer showing the linear frequency dispersion for out-of-plane applied fields; (b) Out-of-plane resonance field versus frequency for a 1.4 nm and a 2.0 nm CoFeB split layer, where the lines reflect fitting the Kittel equation to the data (open markers); (c) Same as in (b) for planar applied magnetic fields; and (d) out-of-plane linewidth versus frequency for a 1.4 nm and a 2.0 nm thick CoFeB split layer.

Ta dusting layer. Additionally, the increased damping in the case of the 1.4 nm thick sample could be attributed to the enhanced spin relaxation due to spin-orbit coupling. Also, an increase in damping has been reported upon crystallization of the Ta/CoFeB/MgO stacks [35] – 1 nm thick amorphous $\text{Co}_{20}\text{Fe}_{60}\text{B}_{20}$ layer were found to have α equal to 0.014, whereas increases to 0.015 after annealing – suggesting a crystalline structure of our split-CoFeB layers.

Besides g -factor and damping, the effective magnetic anisotropy is obtained from FMR measurements and reported here. A $\mu_0 H_{\text{eff}}$ value of 0.57 T is obtained for the annealed split-CoFeB layer with 1.4 nm thickness. A much lower value of 0.36 T is obtained for the annealed W/Ta/CoFeB/MgO stack with equal thickness characterized during this study (see Supplementary data). Furthermore, the values reported in the literature for Ta/CoFeB/MgO layers of similar thicknesses are also lower: 0.28 T is reported for a 1.3 nm thick layer in [5], whereas 0.43 T is reported for a 1.3 nm thick one in [35]. With the exception of the 1.4 nm-thick split-CoFeB layer, all samples show $\mu_0 H_{\text{eff}}^{\parallel} > \mu_0 H_{\text{eff}}^{\perp}$, suggesting that the fourth-order anisotropy strength is negative

($2K_4/M_S < 0$). Furthermore, this negative contribution tends to increase with increasing thickness, reaching a maximum of $-0.136 \text{ T} \pm 0.008 \text{ T}$ in the annealed W/Ta/CoFeB (2.0 nm)/MgO film. This indicates that besides higher magnetization, the split-CoFeB design allows also for obtaining higher magnetic anisotropy energy.

4. Conclusions

To summarize, we have studied the static and dynamic magnetic properties of split-CoFeB layers grown on β -W. Split-CoFeB layers show higher tendency to promote PMA, compared to W/Ta/CoFeB/MgO stacks deposited under identical conditions; PMA is obtained even at the as-deposited state and the PMA to IMA transition occurs at 1.7 nm (1.8 nm) before (after) annealing. Also, saturation magnetization is higher at the split-CoFeB layers (1440 kA/m), compared to non-split ones (1200 kA/m). Gilbert damping was found to be higher in the case of the split-CoFeB layers, although the obtained values are moderate (0.030 at a 1.4 nm thick split-CoFeB layer) and they are combined to an

Table 1

Magnetic properties obtained from FMR: effective magnetic anisotropy field, gyromagnetic ratio (g) obtained from perpendicular (\perp) and in-plane (\parallel) measurements, and Gilbert damping factor (α) of split-CoFeB and W/Ta/CoFeB/MgO stacks. Uncertainty in our best-fit parameters comprises the standard uncertainty from a least-squares fit to the Kittel equation and uncertainty in the measured applied external field.

Sample	$\mu_0 H_{\text{eff}}^{\perp}$ (T)	$\mu_0 H_{\text{eff}}^{\parallel}$ (T)	g	α
Split-CoFeB 1.4 nm	0.571 ± 0.003	0.546 ± 0.004	2.22 ± 0.03 (\perp)	0.030 ± 0.001
			1.94 ± 0.01 (\parallel)	
Split-CoFeB 2.0 nm	-0.165 ± 0.003	-0.085 ± 0.002	2.10 ± 0.02 (\perp)	0.021 ± 0.002
			2.10 ± 0.03 (\parallel)	
CoFeB 1.4 nm	0.362 ± 0.004	0.410 ± 0.005	2.12 ± 0.02 (\perp)	0.022 ± 0.002
			2.00 ± 0.02 (\parallel)	
CoFeB 1.8 nm	-0.626 ± 0.003	-0.490 ± 0.005	2.03 ± 0.01 (\perp)	0.032 ± 0.001
			2.11 ± 0.02 (\parallel)	

effective magnetic anisotropy field of 0.571 T. In conclusion, CoFeB/Ta/CoFeB split layers deposited onto β -W underlayers combine a high effective magnetic anisotropy field and moderate Gilbert damping, making those more promising for devices, compared to similarly prepared continuous CoFeB layers. Drop-in values for the saturation magnetization, dead layer thickness, magnetic anisotropy, Gilbert damping, and spectroscopic-g factor are also provided. We believe that this work can guide future device simulation and fabrication for emerging spin-orbit-torque magnetic memory applications.

The [Supplementary Material](#) section includes additional VSM and FMR measurements and analysis of samples, including additional sample series.

Acknowledgements

Funding from the EC (Grant No. 318144 and 686056), from the Spanish MINECO (ref. MAT2014-59772-C2-1-P) and from Comunidad de Madrid (Nanofrontmag, ref. P2013/MIT-2850), is acknowledged.

Appendix A. Supplementary data

Supplementary data to this article can be found online at <https://doi.org/10.1016/j.jmmm.2018.10.103>.

References

- [1] J. Torrejon, J. Kim, J. Sinha, S. Mitani, M. Hayashi, M. Yamanouchi, H. Ohno, *Nat. Commun.* 5 (2014) 4655.
- [2] Q. Hao, G. Xiao, *Phys. Rev. Appl.* 3 (2015) 034009.
- [3] H. Almasi, C.L. Sun, X. Li, T. Newhouse-Illige, C. Bi, K.C. Price, S. Nahar, C. Grezes, Q. Hu, P. Khalili Amiri, K.L. Wang, P.M. Voyles, W.G. Wang, *J. Appl. Phys.* 121 (2017) 153902.
- [4] M. Wang, W. Cai, K. Cao, J. Zhou, J. Wrona, S. Peng, H. Yang, J. Wei, W. Kang, Y. Zhang, J. Langer, B. Ocker, A. Fert, W. Zhao, *Nat. Commun.* 9 (2018) 671.
- [5] S. Ikeda, K. Miura, H. Yamamoto, K. Mizunuma, H.D. Gan, M. Endo, S. Kanai, J. Hayakawa, F. Matsukura, H. Ohno, *Nat. Mater.* 9 (2010) 721.
- [6] I.M. Miron, K. Garello, G. Gaudin, P.J. Zermatten, M.V. Costache, S. Auffret, S. Bandiera, B. Rodmacq, A. Schuhl, P. Gambardella, *Nature* 476 (2011) 189.
- [7] S. Shi, Y. Ou, S.V. Aradhya, D.C. Ralph, R.A. Buhrman, *Phys. Rev. Appl.* 9 (2018) 011002.
- [8] M. Cubukcu, O. Boule, N. Mikuszeit, C. Hamelin, T. Brächer, N. Lamard, M.-C. Cyrille, L. Buda-Prejbeanu, K. Garello, I.M. Miron, O. Klein, G. de Loubens, V.V. Naletov, J. Langer, B. Ocker, P. Gambardella, G. Gaudin, *IEEE Trans. Mag.* 54 (2018) 9300204.
- [9] Q. Ma, Y. Li, D.B. Gopman, Y.P. Kabanov, R.D. Shull, C.L. Chien, *Phys. Rev. Lett.* 120 (2018) 117703.
- [10] C.F. Pai, L. Liu, Y. Li, H.W. Tseng, D.C. Ralph, R.A. Buhrman, *Appl. Phys. Lett.* 101 (2012) 122404.
- [11] W. Skowronski, T. Nozaki, D.D. Lam, Y. Shiota, K. Yakushiji, H. Kubota, A. Fukushima, S. Yuasa, Y. Suzuki, *Phys. Rev. B* 91 (2015) 184410.
- [12] G.G. An, J.B. Lee, S.M. Yang, J.H. Kim, W.S. Chung, J.P. Hong, *Acta Mater.* 87 (2015) 259.
- [13] Y. Liu, T. Yu, Z. Zhu, H. Zhong, K.M. Khamis, K. Zhu, *J. Magn. Magn. Mat.* 410 (2016) 123.
- [14] D.H. Kim, K.W. Park, B.G. Park, *Curr. Appl. Phys.* 17 (2017) 962.
- [15] C.F. Pai, M.H. Nguyen, C. Belvin, L.H. Vilela-Leao, D.C. Ralph, R.A. Buhrman, *Appl. Phys. Lett.* 104 (2014) 082407.
- [16] A. Kaidatzis, C. Bran, V. Psycharis, M. Vázquez, J.M. García-Martín, D. Niarchos, *Appl. Phys. Lett.* 106 (2015) 262401.
- [17] C. Zhang, S. Fukami, K. Watanabe, A. Ohkawara, S. Dutta Gupta, H. Sato, F. Matsukura, H. Ohno, *Appl. Phys. Lett.* 109 (2016) 192405.
- [18] T. Liu, J.W. Cai, L. Sun, *AIP Adv.* 2 (2012) 032151.
- [19] J.-H. Kim, J.-B. Lee, G.-G. An, S.-M. Yang, W.-S. Chung, H.-S. Park, J.-P. Hong, *Sci. Rep.* 5 (2015) 16903.
- [20] B.D. Clark, S. Paul, S.C. Schwarm, A. Singh, A. Natarajathinam, S. Gupta, *J. Magn. Magn. Mat.* 398 (2016) 54.
- [21] G.Y. Shi, C.H. Wan, Y.S. Chang, F. Li, X.J. Zhou, P.X. Zhang, J.W. Cai, X.F. Han, F. Pan, C. Song, *Phys. Rev. B* 95 (2017) 104435.
- [22] C. Bi, H. Almasi, K. Price, T. Newhouse-Illige, M. Xu, S.R. Allen, X. Fan, W. Wang, *Phys. Rev. B* 95 (2017) 104434.
- [23] S. Yuasa, D.D. Djayaprawira, *J. Phys. D: Appl. Phys.* 40 (2007) R337.
- [24] A. Kaidatzis, V. Psycharis, J.M. García-Martín, C. Bran, M. Vázquez, D. Niarchos, *Mater. Res. Soc. Symp. Proc.* 1729 (2015) 101557.
- [25] A. Kaidatzis, V. Psycharis, K. Mergia, D. Niarchos, *Thin Solid Films* 619 (2016) 61.
- [26] M.T. Johnson, P.J.H. Bloemen, F.J.A. den Broeder, J.J. de Vries, *Rep. Prog. Phys.* 59 (1996) 1409–1458.
- [27] S.Y. Jang, C.-Y. You, S.H. Lim, S.R. Lee, *J. Appl. Phys.* 109 (2011) 013901.
- [28] P. Khalili Amiri, Z.M. Zeng, J. Langer, H. Zhao, G. Rowlands, Y.-J. Chen, I.N. Krivorotov, J.-P. Wang, H.W. Jiang, J.A. Katine, Y. Huai, K. Galatsis, K.L. Wang, *Appl. Phys. Lett.* 98 (2011) 112507.
- [29] P.G. Gowtham, G.M. Stiehl, D.C. Ralph, R.A. Buhrman, *Phys. Rev. B* 93 (2016) 024404.
- [30] M. Farle, *Rep. Prog. Phys.* 61 (1998) 755–826.
- [31] C.E. Patton, Z. Frait, C.H. Wilts, *J. Appl. Phys.* 46 (1975) 5002.
- [32] A.J. Lee, J.T. Brangham, Y. Cheng, S.P. White, W.T. Ruane, B.D. Esser, W.D. McComb, P.C. Hammel, F. Yang, *Nat. Comm.* 8 (2017) 234.
- [33] F. Schreiber, J. Pflaum, Z. Frait, Th. Miihge, J. Pelzl, *Solid State Commun.* 93 (1995) 965.
- [34] J.M. Shaw, H.T. Nembach, M. Weiler, T.J. Silva, M. Schoen, J.Z. Sun, D.C. Worledge, *IEEE Magn. Lett.* 6 (2015) 3500404.
- [35] T. Devolder, P.H. Ducrot, J.P. Adam, I. Barisic, N. Vernier, J.V. Kim, B. Ockert, D. Ravelosona, *Appl. Phys. Lett.* 102 (2013) 022407.

A. Kaidatzis^{a,*}, D.B. Gopman^b, C. Bran^c, J.M. García-Martín^d, M. Vázquez^c, D. Niarchos^a

^a Institute of Nanoscience and Nanotechnology, NCSR Demokritos, 153 10, Aghia Paraskevi, Athens, Greece

^b Materials Science and Engineering Division, National Institute of Standards and Technology, 100 Bureau Dr., Gaithersburg, MD 20899, USA

^c ICMM-Instituto de Ciencia de Materiales (ICMM-CSIC), Sor Juana Inés de la Cruz 3, E-28049 Cantoblanco, Madrid, Spain

^d Instituto de Micro y Nanotecnología IMN-CNM, CSIC, CEI UAM + CSIC, Calle Isaac Newton 8, Tres Cantos, 28760 Madrid, Spain
E-mail address: a.kaidatzis@inn.demokritos.gr (A. Kaidatzis)

* Corresponding author.